

# On the Heat Capacity of Pure Elements and Phases

Ivaldo Leão Ferreira<sup>a</sup> 

<sup>a</sup>Universidade Federal do Pará, Faculdade de Engenharia Mecânica, Augusto Corrêa Avenue 1, 66075-110, Belém, PA, Brasil

Received: November 18, 2020; Revised: January 12, 2021; Accepted: January 26, 2021

Recently, a model was proposed to predict  $c_v$  as a function of temperature from the absolute zero to the melting temperature applied. This solution was based on critical grain nucleation to determine the volume, which contains the total number of modes for a particular equilibrium and non-equilibrium state to calculate the density of state (DoS), which is strongly dependent on the nucleus radius for both pure element and compound. Electronic and rotational energies were regarded for both elements and compounds in this formulation. The anomalies associated with  $c_v$  can be easily considered in terms of their entropies, independent of their nature, as a local change in the DoS. Comparisons of  $c_v$  for elements and compounds are performed against Thermodynamics software simulations and experimental data.

*Keywords: Molar heat capacity, Density of State, Elements and compounds, Computational Thermodynamics, Anomalies of heat capacity.*

## 1. Introduction

The molar heat capacity for the solid-state of matter is important thermophysical properties for many branches of physics and engineering. There are two methods available for its calculation: (i) for high temperatures, in which empirical formulae based on integrals and experimental coefficients are normally used to calculate the molar specific heat as a polynomial function of temperature<sup>1</sup> and (ii) with the use of Computational Thermodynamics packages and databases to be numerically determined for a specific class of materials<sup>2</sup>. For lower temperatures, the realm of the quantum pronounced effects, historically, Einstein<sup>3</sup> modeled the atoms in a solid as independent harmonic oscillators vibrating at the same frequency, thereby modeling the density of state as a delta function. This simple density of state sometimes provides a good correlation with experimental heat capacity measurements at high temperatures, failing at low temperatures. Debye<sup>4,5</sup> otherwise modeled the vibrations in a solid as normal modes of a continuous elastic body, which corroborates well for long-wavelength vibrations that do not depend on the detailed atomic character of the solid and do conform better experimental scatter to lower temperatures, but failing for many materials with a gap in the density of state<sup>6,7</sup>. Another approach is applying *ab initio* calculations to predict several thermodynamics properties and the molar heat capacity<sup>8,9</sup>. Debye's model does not consider rotational<sup>10</sup>, electronic<sup>11</sup>, and magnetic<sup>12-14</sup> energies contributions to the molar specific heat. The magnetic contribution to the molar heat capacity usually is empirical formulae to account for contributions of Curie, Neel, and Schottky transition anomalies<sup>15</sup>. They calculated the Gibbs-Thomson coefficient for the equilibrium and the non-equilibrium solidification of Al-Cu-Si-Mg alloys as a function of Si content. By observing a different set of Gibbs-Thomson coefficients values for equilibrium and non-

equilibrium conditions, they defined this coefficient for alloy by the limiting case<sup>16</sup>. Ferreira et al.<sup>17</sup> derived a model for pure elements and compounds, regarding the critical radius expressed in terms of the temperature drop ( $\Delta T(r)$ ) by means of the correlation between the solid-liquid surface tension ( $\sigma_{sl}$ ) and the bulk melting entropy by unit volume ( $\Delta S_v$ ), which writes in terms of the Gibbs-Thomson coefficient ( $\bar{A}$ ). Consequently, a relation between bulk lattice and the surface lattice interatomic spacings, i.e., the reciprocal lattice in both networks and density of state (DoS), and the total number of atoms in the volume and a correspondent density of atoms  $n$  limited by nucleation conditions were proposed. Authors regarded the electronic and rotational energies contributions to the molar heat capacity ( $c_v$ ).

In this paper, calculations are performed for molar heat capacities of pure elements and phases, compared with the Thermo-Calc Software simulations and with experimental data.

## 2. Numerical Approach and Analytical Models

The thermal energy of materials is stored in several forms, such as translational, vibrational, rotational, electronic, and magnetic. In a solid element and compound, the translational contribution can be neglected<sup>10</sup>. The magnetic anomalies are generally modeled empirically<sup>11-15</sup>. Considering all contributions to the thermal heat capacity, it provides,

$$c_v = c_v^{Trans} + c_v^{Vib} + c_v^{Rot} + c_v^e + c_v^{Mag} \quad (1)$$

In this paper, applying Equation 1 to a solid element or compound, and the discussion about the magnetic contribution  $c_v^{Mag}$  is postponed. By now, the thermal molar heat capacity expressed in terms of its components is given by

$$c_v = c_v^{Vib} + c_v^{Rot} + c_v^e \quad (2)$$

\*e-mail: ileao@ufpa.br

The Gibbs-Thomson coefficient describes for pure elements the melting temperature depression  $\Delta T_m [K]$ , based on the solid-liquid interface tension  $\sigma_{sl} [N.m^{-1}]$  and on bulk melting entropy by unit volume  $\Delta S_v [J.K^{-1}.m^{-3}]$ . The Gibbs-Thomson is responsible for the effect of melting temperature drop<sup>6,7</sup>, which is associated with the surface free energy, due to elements bonds in the surface presenting a larger lattice interatomic spacing concerning that of the bulk. Let's consider an isolated solid particle of diameter  $d$  in its liquid, the Gibbs-Thomson equation for the structural melting point depression can be expressed by<sup>16</sup>:

$$\Delta T_m(d) = \frac{4\gamma_{sl} T_m^{bulk}}{\Delta H_v d} = n \frac{4\gamma_{sl}}{\Delta S_v d} \zeta \cong \frac{\sigma_{sl}}{\gamma_{sl}} \frac{4\gamma_{sl}}{\Delta S_v d} \zeta \cong \frac{4\sigma_{sl}}{\Delta S_v d} \zeta \cong \frac{4\Gamma}{d} \zeta \quad (3)$$

where  $n$  and  $\zeta$  are surface energy/surface tension relation parameters associated with the knowledge that crystals exhibit a surface stress that gives rise to small but detectable strains in the interior of the crystal, assumed as  $\zeta = l[m]$  and  $n = \frac{\sigma_{sl}}{\gamma_{sl}}$ ,  $T_m^{bulk}$  is the bulk melting temperature  $[K]$ ,  $\Delta H_v$  is the latent heat of melting per unit volume  $[J.m^{-3}]$  and  $d$  is the spherical solid-phase diameter  $[m]$ , respectively.

According to the definition presented, the Gibbs-Thomson coefficient  $\Gamma$  can be expressed as,

$$\Gamma = \frac{\sigma_{sl}}{\Delta S_v} = \frac{\sigma_{sl} T_m^{bulk}}{\Delta H_v} \quad (4)$$

The same does not occur to alloys. Jácome et al.<sup>18</sup>, while applying several microstructural evolution models for cellular and dendritic growth to binary aluminum alloys, concluded that the Gibbs-Thomson of the solvent was not adequate to predict the evolution of high solute content alloys. Consider an alloy given by Al-50at%Ni, which one solvent,  $\Gamma^{Al}$  or  $\Gamma^{Ni}$  should be adequate to be carried out in the microstructural evolution models? They provide different results for the primary and secondary dendrite arm spacing. Consequently, the authors defined the alloy Gibbs-Thomson coefficient  $\Gamma^{Eq}$  able to encompass the full range of alloy concentration,

$$\Gamma^{Eq} = \frac{\sigma_{sl}}{\Delta S_v^{Eq}} = \frac{\sigma_{sl} T_L^{bulk}}{\Delta H_v^{Eq}} \quad (5)$$

where  $\sigma_{sl}$  is the alloy solid-liquid surface tension,  $\Delta S_v^{Eq}$  and the alloy solidification entropy,  $T_L^{bulk}$  is the liquidus temperature, and finally,  $\Delta H_v^{Eq}$  is the alloy latent heat per unit volume  $[J.m^{-3}]$ .

As alloy solidification hardly occurs in equilibrium governed by the Lever Rule or in absolute non-equilibrium by the absence of solute back-diffusion in solid governed by the Scheil equation. Many authors contributed to the estimation and calculation of back-diffusion parameter  $\beta$ . In 1981, Clyne and Kurz<sup>19</sup> derived an approximate relation,

$$\beta = 2\alpha \left(1 - e^{-l/\alpha}\right) - e^{-l/2\alpha} \quad (6)$$

where  $\alpha$  is the standard Fourier diffusion number. This proposed back diffusion treatment uses the Clyne and

Kurz<sup>19</sup> correction of the Brody and Flemings<sup>20</sup>. In 2001, a general and exact description of the back-diffusion parameter was derived, according to Voller<sup>21</sup>. The model used in this paper to calculate the back-diffusion parameter  $\beta$  is the one derived by Voller.

What is the connection between equilibrium and non-equilibrium solidification for alloy the Gibbs-Thomson coefficient? It's common knowledge that in the equilibrium solidification, higher latent heat is expected when compared to that in non-equilibrium conditions, as demonstrated in the work of Ferreira and Garcia<sup>16</sup> and presented in Figure 1 for the alloys example above.

Figure 1 shows heat and latent heat per gram as a function of the temperature solidification range. The curve corresponding to the highest values of heat is associate with infinite diffusion in solid. The lowest curve represents the absence of back-diffusion in the solid phase. Between the curves is the so-called finite back-diffusion condition<sup>19,21</sup>.

In 2019, Ferreira and Garcia<sup>16</sup> calculated the Gibbs-Thomson coefficient for the equilibrium and the non-equilibrium solidification of Al-Cu-Si-Mg alloys as a function of Si content. By observing a different set of Gibbs-Thomson coefficients values for equilibrium and non-equilibrium conditions, they defined this coefficient for alloy by the limiting case. Expecting a greater undercooling for non-equilibrium solidification conditions. Under infinite diffusion in the solid ( $\beta = 1$ ) and no-back-diffusion in the solid ( $\beta = 0$ )

$$\Gamma^{Eq} = \frac{\sigma_{sl}}{\Delta S_v^{Eq}} = \frac{\sigma_{sl} T_m^{bulk}}{\Delta H_v^{Eq}} \quad (7a)$$

$$\Delta T^{Eq}(d) = \frac{4\Gamma^{Eq}}{d} \quad (7b)$$

and a non-equilibrium one as,

$$\Gamma^{Non-Eq} = \frac{\sigma_{sl}}{\Delta S_v^{Non-Eq}} = \frac{\sigma_{sl} T_m^{bulk}}{\Delta H_v^{Non-Eq}} \quad (8a)$$

$$\Delta T^{Non-Eq}(d) = \frac{4\Gamma^{Non-Eq}}{d} \quad (8b)$$

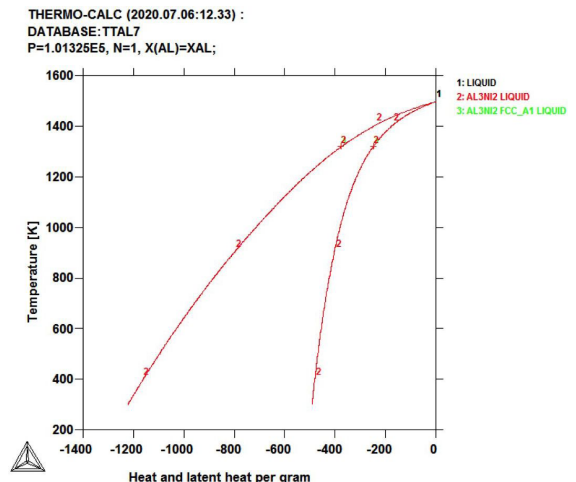


**Figure 1.** Equilibrium and non-equilibrium latent heat and latent heat per gram as a function of temperature for Al-50at%Ni.

Ferreira and Garcia<sup>16</sup> assumed the solid-solid phase nucleation, based on several observations of equilibrated boundary groove shapes at multiple crystallographic orientations influencing the crystal-melt interfacial energy<sup>22,23</sup>, where the Gibbs-Thomson coefficient definition could be generalized for solid-phase transformations by carrying out the grain boundary surface tension  $\sigma_{GB}$  to predict the solid phase transformation temperature drop  $\Delta T_T(d)$ , that is,

$$\Gamma_T^{SPT Eq} = \frac{\sigma_{GB}}{\Delta S_{\nabla}^{SPT Non}} = \frac{\sigma_{GB} T_T^{bulk}}{\Delta H_{\nabla}^{SPT Non}} \quad (9a)$$

$$\Delta T_T^{SPT Eq}(d) \approx \frac{4\Gamma_T^{Eq}}{d} \quad (9b)$$

and,

$$\Gamma_T^{SPT Non-Eq} = \frac{\sigma_{GB}}{\Delta S_{\nabla}^{SPT Non-Eq}} = \frac{\sigma_{GB} T_T^{bulk}}{\Delta H_{\nabla}^{SPT Non-Eq}} \quad (10a)$$

$$\Delta T_T(d) \approx \frac{4\Gamma_T^{SPT Non-Eq}}{d} \quad (10b)$$

where,  $\Gamma_T^{Eq}$  and  $\Gamma_T^{Non-Eq}$  is the Gibbs-Thomson coefficient of equilibrium and non-equilibrium solid phase transformation [ $K.m$ ],  $\sigma_{GB}$  is the interface tension of the grain-boundary [ $N.m^{-1}$ ],  $\Delta S_{\nabla}^{SPT Eq}$  and  $\Delta S_{\nabla}^{SPT Non-Eq}$  are the bulk effective entropies of the solid phase transformation per unit volume for the equilibrium and non-equilibrium in [ $J.m^{-3}.K^{-1}$ ], respectively.  $\Delta H_{\nabla}^{SPT Eq}$  and  $\Delta H_{\nabla}^{SPT Non-Eq}$  are the bulk heats of the solid phase transformation per unit volume [ $J.m^{-3}$ ] for the equilibrium and non-equilibrium conditions, respectively.  $T_T^{bulk}$  is the bulk solid transformation temperature [ $K$ ]. The eutectic and eutectoid reactions are both examples of such solid transformations. The grain boundary surface tension  $\sigma_{GB}$  is greater than the solid/liquid surface  $\sigma_{sl}$ , as far as the solid-solid interface barrier energy for the nucleation of a new solid phase is greater than that of the solid-liquid.

In the case of an element, for a given nucleus to be stable and to grow, it must have at least a radius  $r$  greater than or even equal to the critical radius  $r_C$ , i.e.,  $r \geq r_C$ . This critical radius can be expressed in terms of the temperature drop  $\Delta T(r)$  through the correlation between the solid-liquid surface tension  $\sigma_{sl}$  and the bulk melting entropy by unit volume  $\Delta S_{\nabla}$ , which can be written in terms of the Gibbs-Thomson coefficient  $\dot{\lambda}$ .

$$\Delta T(r \geq r_C) = \frac{2\Gamma}{r} \quad (11)$$

There is a relation between bulk lattice and the surface network parameters. Consequently, the reciprocal lattice in both networks and density of state (DoS) which is dependent on the nucleus radius. The density of state  $D(\omega)$  for a given grain of volume  $\nabla$  regarding the critical nucleation radius, is defined as

$$D(\omega) = \frac{\nabla \omega^2}{2\pi^2 v^3} \quad (12)$$

where  $\omega$  is the frequency,  $v$  is the speed of sound in the solid phase. For a total number of atoms  $N$  in the volume  $\nabla$  and a correspondent density of atoms  $n$ , these variables can be expressed as,

$$N = n \nabla \quad (13)$$

The first Brillouin zone is exchanged by an integral over a sphere of radius  $k_D$ , containing precisely  $N$  wave vectors allowed. As a volume of space  $k$  by wave vector is e requires,

$$\frac{(2\pi)^3}{\nabla} N = \frac{4\pi k_D^3}{3} \quad (14)$$

Then, the density of atoms  $n$  can be obtained as,

$$n = \frac{k_D^3}{6\pi^2} = \frac{l}{6\pi^2} \left( \frac{k_B \Theta_D}{h\nu} \right)^3 \quad (15)$$

As observed in Equation 15, the compound fundamental frequencies are expressed as a function of the linear combination of Debye's temperatures of elements  $i$ , that is,

$$\omega_D = \frac{k_B \cdot \Theta_D}{h} \quad (16)$$

where,  $\Theta_D$  is the Debye's temperature of element  $i$ ,  $k_B$  and  $h$  are the constant of Boltzmann and Planck, respectively.

The electronic contribution to  $c_{ve}$  is written in terms of the phonon energy  $c_v^{Vib}$  as the following,

$$\frac{c_{ve}}{c_v^{Vib}} = \frac{5}{24\pi^3} Z \frac{\Theta_D^3}{T^2 T_m^{bulk}} \quad (17)$$

where,  $z$  is the valence of the element,  $T_m^{bulk}$  is the melting temperature of element [ $K$ ] and  $T$  is the absolute temperature [ $K$ ].

In 2019, Ferreira et al.<sup>17</sup> considered the following approach for the rotational energy,

$$E_{Rot} = \frac{5}{4} \hbar^2 \frac{J(J+1)}{\bar{M} \cdot r^2} [J] \quad (18)$$

where,  $J$  is the rotational level corresponding to integer  $J = 0, 1, 2, 3, \dots, r$  and  $\bar{M}$  are the atomic radius and the molar mass, respectively. The rotational contribution  $c_v^{Rot}$  to molar heat capacity can be derived as,

$$c_v^{Rot} = \frac{5}{4} \frac{R \cdot \hbar^3}{k_B^2 \omega_D (T + \Theta_D)^2} \frac{J(J+1)}{\bar{M} \cdot r^2} [J.mol^{-1}.K^{-1}] \quad (19)$$

where,  $R$  is the universal gas constant [ $J.mol^{-1}.K^{-1}$ ],  $\omega_D$  is the maximum admissible frequency known as Debye's frequency.

Debye's temperature for pure elements is typically found in the literature<sup>5</sup>. The Equation 17 addition of the electronic and Equation 19 of the rotational contributions to  $c_v$ , it provides,

$$c_v = (1.0 + D(\omega)) 9 N_a k_B \left( \frac{T}{\bar{E}_D} \right)^3 \frac{\bar{E}_D}{T} \int_0^{\frac{T}{\bar{E}_D}} \frac{x^4 e^x}{(e^x - 1)^2} dx (1 + c_{ve}) + (n + 1/2) \left[ 9.0 c_v^{Rot} + \left( 1 - \sqrt{\frac{E \cdot \rho_{Dia}}{E_{Dia} \cdot \rho}} \right) \frac{RT^3}{\bar{E}_D T_m^2} \right] \quad (20)$$

Let's analyze the effects of surface and the bulk reciprocal lattices, for a grain of radius greater than the critical concerning the Brillouin zone, whose reciprocal lattice do not coincide for bulk and surface, due to atoms arrangement in both lattices. Another important aspect is the difference in the solute concentration in the bulk and in the surface regions that contributes to change the reciprocal lattice.

The density of state  $D_{Comp}(\omega_{Comp})$  for a grain of a compound of volume  $\forall$ , with a certain critical nucleation radius is defined as

$$D_{Comp}(\omega_{Comp}) = \frac{\forall \omega_{Comp}^2}{2\pi^2 \nu^3} \quad (21)$$

where  $\omega_{Comp}$  is the frequency,  $\nu$  is the speed of sound in the solid compound. For a total number of atoms  $N$  in the volume  $\forall$  and a correspondent density of atoms  $n$ , these variables can be expressed as

$$N = n\forall \quad (22)$$

The first Brillouin zone is exchanged by an integral over a sphere of radius  $k_D$ , containing precisely  $N$  wave vectors allowed. As a volume of space  $k$  by wave vector is  $e$  requires

$$\frac{(2\pi)^3}{\forall} N = \frac{4\pi k_D^3}{3} \quad (23)$$

Then, the density of atoms  $n$  can be obtained as

$$n = \frac{k_D^3}{6\pi^2} = \frac{1}{6\pi^2} \left( \frac{k_B \Theta_{D,Comp}}{\hbar \nu} \right)^3 \quad (24)$$

and,

$$\Theta_{D,Comp} = \sum_{i=1}^n x_i \Theta_{D,i} \quad (25)$$

As observed in Equation 14, the compound fundamental frequencies are expressed as a function of the linear combination of Debye's temperatures of elements  $i$ , that is,

$$\omega_{D,Comp} = \frac{k_B \cdot \Theta_{D,Comp}}{\hbar} \quad (26)$$

where,  $\Theta_{D,i}$  is the Debye's temperature of element  $i$ ,  $\Theta_{D,Comp}$  is the compound Debye's temperature,  $k_B$  and  $\hbar$  are the constant of Boltzmann and Planck, respectively.

The undercooling for a critical grain of a volume  $\forall$  can be written for solid-liquid nucleation

$$\Gamma_{Comp} = \frac{\sigma_{sl}^{Comp}}{\Delta S_{\forall}^{Comp}} = \frac{\sigma_{sl} T_L^{bulk}}{\Delta H_{\forall}^{Comp}} \quad (27a)$$

$$\Delta T(r_C) = \frac{2\Gamma_{Comp}}{r_C} \quad (27b)$$

and for solid-solid nucleation as

$$\Gamma_G^{Comp} = \frac{\sigma_{GB}^{Comp}}{\Delta S_{\forall}^{Comp}} = \frac{\sigma_{GB} T_T^{bulk}}{\Delta H_{\forall}^{Comp}} \quad (27c)$$

$$\Delta T(r_{CG}) = \frac{2\Gamma_T^{Comp}}{r_{CG}} \quad (27d)$$

where,  $\Gamma_{Comp}$  is the solid-liquid nucleation Gibbs-Thomson coefficient  $[K.m]$ ,  $\Gamma_G^{Comp}$  is the solid-solid nucleation Gibbs-Thomson coefficient  $[K.m]$ ,  $r_C$  is the critical solid-liquid nucleation grain radius  $[m]$ ,  $r_{CG}$  is the critical solid-solid nucleation grain radius  $[m]$ .

The element  $i$  electronic contribution to  $c_{ve}$  is written in terms of the phonon energy  $c_v^{Vib}$  as the following,

$$\frac{c_{ve,i}}{c_v^{Vib}} = \frac{5}{24\pi^3} Z_i \frac{\Theta_{D,i}^3}{T^2 T_{m,i}^{bulk}} \quad (28)$$

where,  $Z_i$  is the valence of element  $i$ ,  $T_{m,i}^{bulk}$  is the melting temperature of element  $i$   $[K]$  and  $T$  is the absolute temperature  $[K]$ .

Thus, the total electronic contribution  $c_{ve,i}$  to the electronic molar heat capacity  $c_{ve,Comp}$  can be expressed as

$$c_{ve,Comp} = \sum_{i=1}^n x_i \cdot c_{ve,i} + \sum_{i=1}^n \sum_{j>i} x_j \cdot x_i \cdot c_{ve,i} \cdot c_{ve,j} + \prod_{i=1}^n x_i \cdot c_{ve,i} \quad (29)$$

where,  $x_i$  is the molar fraction of element  $i$ .

In 2019, Ferreira et al.<sup>17</sup>, regarded the following approach for the rotational energy for each element  $i$ ,

$$E_{Rot,i} = \frac{5}{4} \hbar^2 \frac{J_i(J_i+1)}{\bar{M}_i \cdot r_i^2} [J] \quad (30)$$

where,  $J_i$  is the rotational level corresponding to integer  $J=0,1,2,3,\dots$ ,  $r_i$  and  $\bar{M}_i$  are the atomic radius and the molar mass of element  $i$ , respectively. The rotational contribution  $c_v^{Rot}$  to molar heat capacity can be derived as,

$$c_v^{Rot} = \frac{5}{4} \frac{R \cdot \hbar^3}{k_B^2 \omega_{D,Comp} (T + \Theta_{D,Comp})^2} \sum_{i=1}^n \frac{x_i \cdot J_i(J_i+1)}{\bar{M}_i \cdot r_i^2} [J.mol^{-1}.K^{-1}] \quad (31)$$

where,  $R$  is the universal gas constant  $[J.mol^{-1}.K^{-1}]$ ,  $\omega_{D,Comp}$  is the maximum admissible frequency known as Debye's frequency.

The modified Debye's equation for compounds is derived on the Neumann-Koop principal. In this model proposed by Ferreira et al.<sup>17</sup>, the Authors neglected magnetic anomalies such as Curie, Neel, and Schottky. The obtained final equation molar heat capacity for a compound is given by,

$$c_v = (1.0 + D_{Comp}(\omega_{Comp})) 9 N_A k_B \left( \frac{T}{E_{D,Comp}} \right)^3 \int_0^{\frac{T}{E_{D,Comp}}} \frac{x^4 e^x}{(e^x - 1)^2} dx (1 + c_{ve}) + \quad (32)$$

$$(n+1/2) \left[ 9.0 c_v^{Rot} + \left( 1 - \sqrt{\frac{E_i D_{Dia}}{E_{D,Alloy} D_i}} \right) \frac{RT^3}{E_{D,Alloy} T_L^2} \right]$$

## 2.1. Magnetic contribution due to anomalies

Specific heat can be characterized by the fundamental excitations involved in the phase transition<sup>24</sup>. According to the authors, phase transitions involving spin, charge, lattice, and orbital degrees of freedom, which under certain circumstances for a given level of lattice thermal vibration associated with special band structure, would define a state of matter, the so-called superconducting state. The concurrence among those phase transitional mechanisms would easily explain how a superconducting state would be achieved at higher temperatures by increasing the pressure<sup>25</sup>, which is

also a variable of state, such as the solute composition<sup>26</sup>. According to Souza et al.<sup>24</sup>, entropy change is associated with a first-order transition, no matter its nature, and can be directly obtained by integrating specific heat over the temperature  $\tau$ . It means that entropy plays the most important role in predicting anomalies. As Ferreira et al.<sup>17</sup> stated the transformation (transitional) entropies change the Density of State  $D(\omega)$ . Consequently, the entropy must be provided, as far as the nucleation entropies of solid-liquid and solid-solid

transformations needed to be provided to determine the critical volume, which encompasses the total number of modes.

### 3. Results and Discussion

The physical properties of elements used to calculate the molar heat capacity are provided in Table 1<sup>5,28</sup>.

Figures 2-5 presents the molar heat capacities for pure Al, Fe, Zr, and Be and the experimental data. Debye's model

**Table 1.** Thermophysical properties of elements.

Properties	Unit	Value
Aluminum Debye's Temperature - $\Theta_{D,Al}$	$K$	433.0
Aluminum latent heat of fusion - $\Delta H_{Al}$	$J.m^{-3}$	397000
Aluminum liquid phase density at the melting point - $\rho_{L,Al}$	$kg.m^{-3}$	2557
Aluminum atomic radius - $r_{Al}$	pm	118
Iron Debye's Temperature - $\Theta_{D,Fe}$	$K$	477.0
Iron latent heat of fusion - $\Delta H_{Fe}$	$J.m^{-3}$	247400
Iron liquid phase density at the melting point - $\rho_{L,Fe}$	$kg.m^{-3}$	7030
Iron atomic radius - $r_{Fe}$	pm	156
Zirconium Debye's Temperature - $\Theta_{D,Zr}$	$K$	290.0
Zirconium latent heat of fusion - $\Delta H_{Zr}$	$J.m^{-3}$	196000
Zirconium liquid phase density at the melting point - $\rho_{L,Zr}$	$V$	6324.4
Zirconium atomic radius - $r_{Zr}$	pm	160
Beryllium Debye's Temperature - $\Theta_{D,Be}$	$K$	981.0
Beryllium latent heat of fusion - $\Delta H_{Be}$	$J.m^{-3}$	1728000
Beryllium liquid phase density at the melting point - $\rho_{L,Be}$	$kg.m^{-3}$	1794.0
Beryllium atomic radius - $r_{Be}$	pm	112.0
Copper Debye's Temperature - $\Theta_{D,Cu}$	$K$	347.0
Copper latent heat of fusion - $\Delta H_{Cu}$	$J.m^{-3}$	209000
Copper liquid phase density at the melting point - $\rho_{L,Cu}$	$kg.m^{-3}$	8125.0
Copper atomic radius - $r_{Cu}$	pm	145.0
Nickel Debye's Temperature <sup>27</sup> - $\Theta_{D,Ni}$	$K$	477.0
Nickel latent heat of fusion - $\Delta H_{Ni}$	$J.m^{-3}$	298500
Nickel liquid phase density at the melting point - $\rho_{L,Ni}$	$kg.m^{-3}$	8237.91
Nickel atomic radius - $r_{Ni}$	pm	149.0
Tellurium Debye's Temperature - $\Theta_{D,Te}$	$K$	153.0
Tellurium atomic radius - $r_{Te}$	pm	138.0
Germanium Debye's Temperature - $\Theta_{D,Ge}$	$K$	371.0
Germanium atomic radius - $r_{Ge}$	pm	122.0
GeTe latent heat of fusion - $\Delta H_{GeTe}$	$J.m^{-3}$	236000.0
GeTe liquid phase density at the melting point - $\rho_{L,GeTe}$	$kg.m^{-3}$	6100
GeTe fusion Temperature - $T_{F,GeTe}$	$K$	998.0
Planck constant - $h$	$J.S$	$6.626 \times 10^{-34}$
Boltzmann constant- $k_B$	$J.K^{-1}$	$1.380658 \times 10^{-23}$
Gas constant - $R$	$J.mol^{-1}.K^{-1}$	8.31451

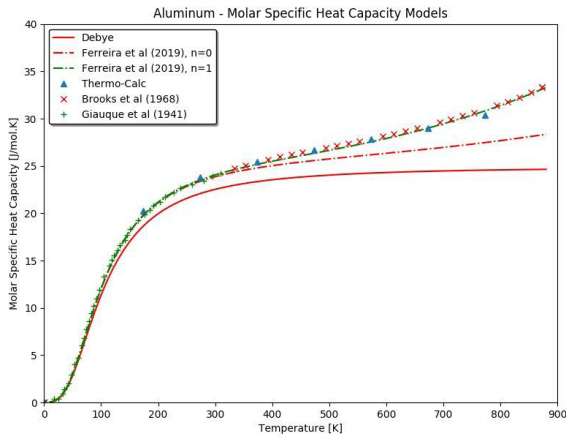


**Figure 2.** Comparison of the molar heat capacity of pure Al by applying Debye, Thermo-Calc, the present approach, and experimental results of Giauque and Meads<sup>29</sup> and Brooks and Bingham<sup>30</sup>.

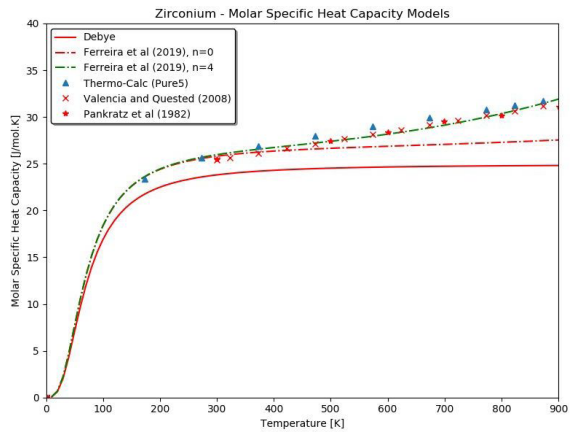


**Figure 4.** Comparison of the molar heat capacity of pure Zr by carrying out Debye, Thermo-Calc, and Ferreira's model.

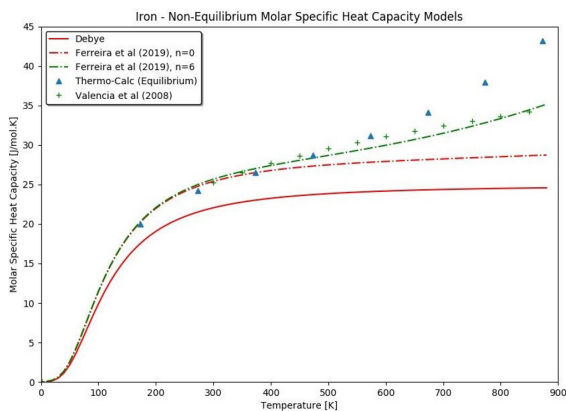
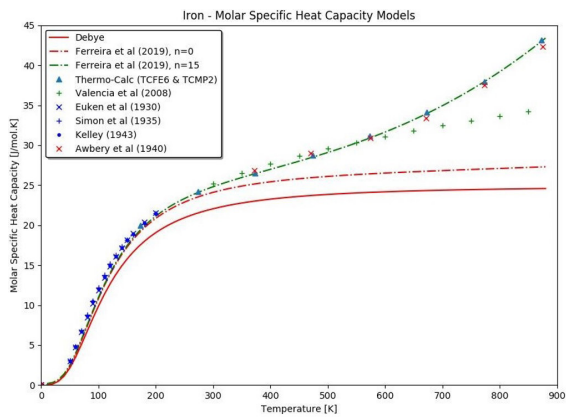


**Figure 3.** Comparison of the molar heat capacity of pure Fe by applying Debye, Thermo-Calc, and Ferreira et al.<sup>17</sup>, and Valencia and Quedsted<sup>31</sup>, (A) equilibrium, and, (B) non-equilibrium.

predictions are present as a reference for Ferreira's model calculations<sup>17</sup>. Instead of using the sound velocities as an approximation for the last term of Equation 21, the value of Young's modulus and the correspondent density was applied to this term. The model proposed<sup>17</sup>, agrees for low and high temperatures with experimental data for Al<sup>29,30</sup>, as far as with Thermo-Calc simulations for equilibrium.

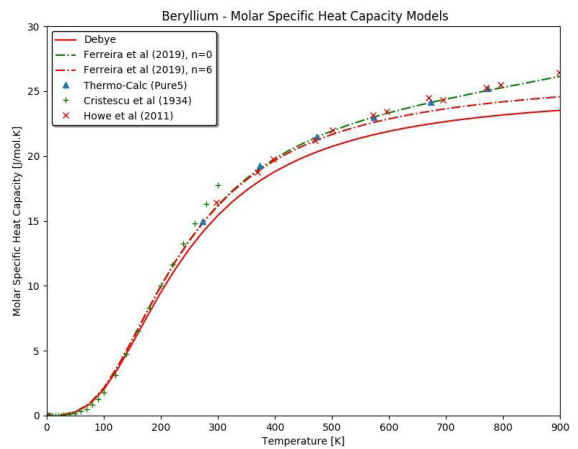


**Figure 5.** Comparison of the molar heat capacity of pure Be by carrying out Debye, Thermo-Calc, Ferreira's model, and experimental data for low-temperature Cristescu and Simon<sup>32</sup> and high-temperature Howe et al.<sup>33</sup>.

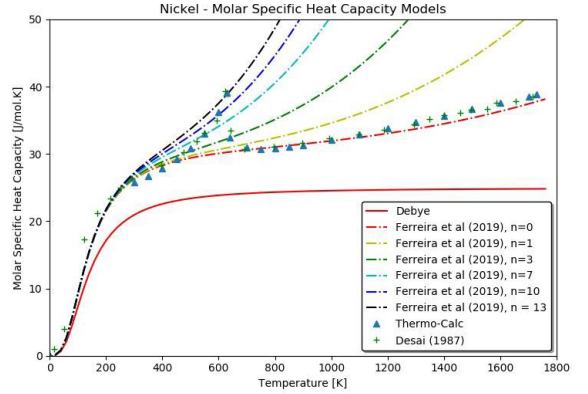
In the case of Fe, equilibrium, and non-equilibrium predictions are shown in Figures 3a and Figure 3b, respectively. For low temperature,  $T \leq 300 K$ , the experimental data are those of Kelley<sup>34</sup>, Euken and Werth<sup>35</sup>, and Simon and Swain<sup>36</sup>. For high temperatures,  $T > 300 K$ , Valencia and Quedsted<sup>31</sup> compiled experimental data from three sources from Smithells<sup>37</sup>, Mills<sup>38</sup>, and Gaskell<sup>39</sup>. The experimental data determined by Awbery and Griffiths<sup>40</sup> fits the Thermo-Calc calculations for the equilibrium condition. In Figure 3a a good agreement is observed for low and high temperatures for all experimental data, Thermo-Calc simulations, and Ferreira's model<sup>17</sup>, except the dataset compilation found in Valencia and Quedsted<sup>31</sup>. As Valencia's compilation dataset provides values below those expected for the equilibrium, it is probably determined under non-equilibrium conditions. Figure 2b presents predictions of Ferreira's model for non-equilibrium conditions, even assuming that a non-equilibrium condition is established since the beginning of data measurements of the three datasets, which is probably not true, Ferreira's model fits the data accordingly.

Figure 4 presents the molar specific heat for Zr as a function of temperature from 0 K to 900 K, for Debye's model, Ferreira's model predictions for fundamental ( $n=0$ ) and fourth ( $n=4$ ) normal modes and Thermo-Calc calculations. The experimental scatter for high temperatures is that found in Pankratz and Mrazek<sup>41</sup>, and Valencia and Quedstedt<sup>31</sup>, whose data is compiled from Smithells<sup>37</sup>. A good agreement can be noticed among the experimental datasets and Ferreira's model calculation.

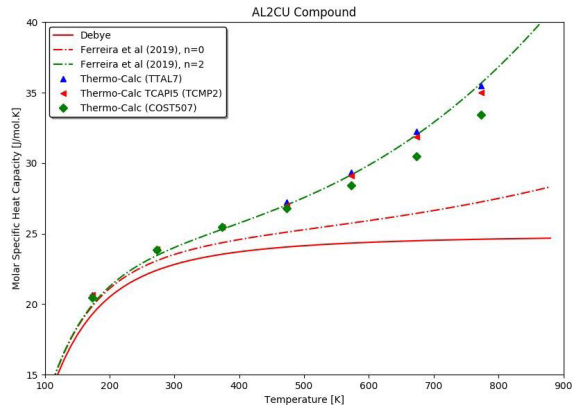
Figure 5 shows the comparison of predictions for molar specific heat capacity considering Ferreira's model and Thermo-Calc. The experiments for low temperature, Cristescu and Simon<sup>32</sup>, and high temperatures, Howe et al.<sup>33</sup> agree with the theoretical predictions of Ferreira's model and Thermo-Calc.

Figure 6 presents the calculation of molar specific heat capacity of pure Nickel as a function of temperature, comparison with Thermo-Calc and, the experimental data found in Desai<sup>42</sup>. The magnetic transition ferromagnetic/paramagnetic of Ni can be captured if the calculation of molar specific heat capacity is performed by the composition of equivalent wavevectors at lattice points  $n$ 's, using  $n = \{0, 1, 3, 7, 10, 13, 10, 7, 3, 1, 0\}$  the model fits the experimental scatter. It seems transformation pass through the sequence of equivalent wavevectors,  $k + 2\pi/a$ , where  $a$  is the lattice spacing at the current temperature, and its anomalies found near the Curie point, as observed by Kohlhaas et al.<sup>43</sup>.

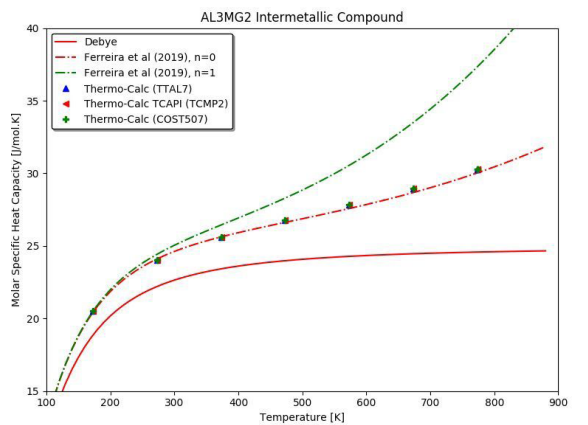
Figures 7-9 present the molar heat capacities for AL2CU, AL3MG2, and AL3Ni2. Debye's model's predictions are present only as a reference for Ferreira's model calculations<sup>17</sup>. Instead of using the sound velocities as an approximation for the last term of Equation 32, the value of Young's modulus and the correspondent density was applied to this term. From the point of view of nucleation of a compound, for a nucleating stable grain concerning the Brillouin zone, another aspect that plays an important role is the difference in the solute concentration in the bulk and the surface regions contributes to change both reciprocal lattices. In the case of the AL2CU phase, calculations are performed by applying Thermo-Calc, and TTAL7 database, Thermo-Calc TCAPIS (Thermo-Calc Application Programming Interface version 5) interface using C++ language routine to perform calculations of specific heat by applying the TCMP2 database, and, finally, Thermo-Calc and COST-507 databases. The first two simulations seem to agree with each other for the whole temperature range. Thermo-Calc using COST-507 seems to deviate from equilibrium but still provides good results slightly. Ferreira's model prediction fits Thermo-Calc and TCAPIS simulations for all databases until temperature reaches 450 K. Beyond, this temperature agrees better with the Thermo-Calc (TTAL7) and TCAPIS (TCMP2) calculations. In Figure 8, calculations were made for the AL3MG2 phase for the equilibrium conditions, where Thermo-Calc, TCAPIS, and Ferreira's model simulations agreed for the whole temperature range. In the AL3Ni2 intermetallic phase, only Thermo-Calc using the TTAL7 database, and TCAPIS routine by utilizing TCMP2 calculation are performed. Ferreira's model results behave equally with the specific molar heat capacity predicted of Thermo-Calc and TCAPIS calculations for the whole range, as shown in Figure 9.



**Figure 6.** Comparison of the molar heat capacity of pure Ni by applying Debye, Thermo-Calc, Ferreira's model, and experimental data from Desai<sup>42</sup>.



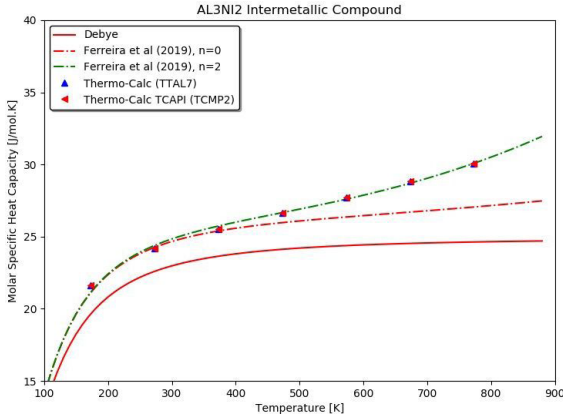
**Figure 7.** Comparison of the molar heat capacity of the AL2CU phase by carrying out Debye, Thermo-Calc, and Thermo-Calc TCAPIS simulations and the Ferreira's model<sup>17</sup>.



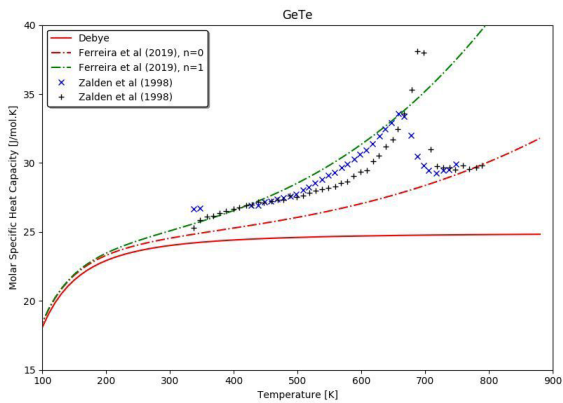
**Figure 8.** Comparison of the molar heat capacity of the AL3MG2 phase by carrying out Debye, Thermo-Calc, and Thermo-Calc TCAPIS simulations and the Ferreira's model<sup>17</sup>.

Figure 10 presents the calculation for the molar specific heat of GeTe compound from 100 to 900 K by applying Ferreira's model and comparing it with two sets of experimental data found in Zalden et al.<sup>28</sup>. A very interesting physical behavior

can be observed, as around 650 K there's a transition from the second ( $n=1$ ) normal mode to the fundamental normal mode ( $n=0$ ) captured by Ferreira's model's predictions.



**Figure 9.** Comparison of the molar heat capacity of the AL3Ni2 phase by carrying out Debye, Thermo-Calc, and Thermo-Calc TCAP15 simulations and Ferreira's model<sup>17</sup>.



**Figure 10.** Comparison of the molar heat capacity of Germanium Telluride (GeTe) by carrying out Debye, Ferreira's model<sup>17</sup>, and experimental data Zalden et al.<sup>28</sup>

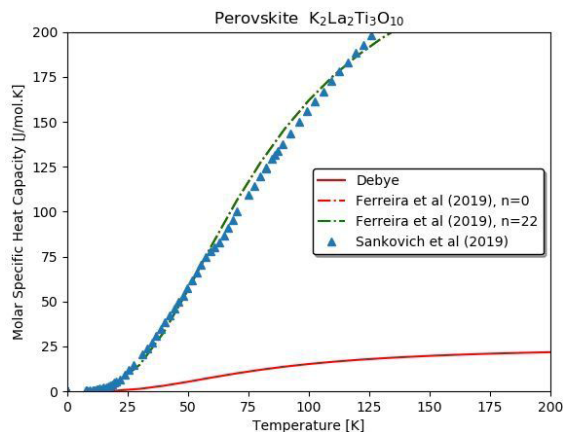


**Figure 11.** Comparison of the molar heat capacity of perovskite  $K_2La_2Ti_3O_{10}$  by carrying out Debye, Ferreira et al.<sup>17</sup> model and first dataset of Sankovich et al.<sup>44</sup>

Calculations with other Pure metals and phases have shown similar behavior.

The critical volume  $v_c$ , of radius  $r \geq r_c$ , which depends on the nucleation kinetics, as demonstrated by Equation 11 and Equation 12, provide the total number of modes  $N$ , under nucleation kinetics restrains. For the lack of nucleation data, the perovskite  $K_2La_2Ti_3O_{10}$  will not be calculated in this paper as many thermophysical properties couldn't be found in the literature. Figure 11 represents only the first dataset of Sankovich et al.<sup>44</sup>.

## 4. Conclusion

The model proposed previously by Ferreira et al.<sup>17</sup> the density of state (DoS) is a function of the nucleation parameters, which influence the reciprocal lattices in the bulk and in the surface of the grain to determine the total number of modes, and consequently, the correct predictions of the Density of State. The model successfully predicts the molar heat capacity's behavior from absolute zero to high temperatures to the melting point for elements and compounds. Furthermore, the formulation encompasses solid-solid grain nucleation, as long as the Gibbs-Thomson coefficient, which is also defined in terms of the solid-solid nucleation, to predict, for instance, the molar specific heat capacity of perlite. A composition of equivalent wavevectors successfully predicted the magnetic transition of Ni. An interesting aspect is the transition mode of the wavevector observed in GeTe, which behavior can also be verified in pure metals, as far as many other substances. The lack of trustworthy thermophysical properties at nucleation temperature (fusion temperature) for perovskite  $K_2La_2Ti_3O_{10}$  did not allow the author to extend the predictions for higher temperatures, as far as Ferreira's model does not have any adjustment parameters, it encompasses only physical properties. Nevertheless, it has predicted the behavior of perovskite's heat capacity correctly where Debye's model fails, as it has no information of the critical volume that contains the total number of modes for a particular equilibrium and non-equilibrium state. Anomalies observed in the molar specific heat capacity, such as thermal, magnetic, configurational transitions, and electronic, can be treated by combining equivalent wavevectors and the Density of State (DoS). This would also explain how the change of other thermodynamic variables of state, such as composition and pressure, can dislocate the superconducting state's critical temperature to higher values.

## 5. Acknowledgments

The authors acknowledge the financial support provided by FAPERJ (The Scientific Research Foundation of the State of Rio de Janeiro), CAPES (Coordenação de Aperfeiçoamento de Pessoal de Nível Superior - Brasil - Finance Code 001) and CNPq (National Council for Scientific and Technological Development).

## 6. References

1. Abu-Eishah SI, Haddad Y, Solieman A, Bajbouj A. A new correlation for the specific heat of metals, metal oxides and metal fluorides as a function of temperature. *Lat Am Appl Res.* 2004;34:257-65.

2. Sundman B, Kattner UR, Sigli C, Stratmann M, Le Tellier R, Palumbo M, et al. The OpenCalphad thermodynamic software interface. *Comput Mater Sci.* 2016;125:188-96.
3. Einstein A. Die plancksche theorie der strahlung und die theorie der spezifischen Wärme. *Ann Phys.* 1907;327(1):180-90.
4. Debye P. Zur theorie der spezifischen Wärmen. *Ann Phys.* 1912;344(14):789-839.
5. Ashcroft NW, Mermin ND. *Solid state physics.* 1. ed. New York: Cengage Learning; 2011. p. 491-598.
6. Schliesser JM, Woodfield BF. Development of a Debye heat capacity model for vibrational modes with a gap in the density of states. *J Phys Condens Matter.* 2015;27(28):285402.
7. Costa EDM, Lemes NHT, Alves MO, Braga JP. Phonon density of states from the experimental heat capacity: an improved distribution function for solid aluminum using an inverse framework. *J Mol Model.* 2014;20(8):2360.
8. DeTar D. Theoretical *ab initio* calculation of entropy, heat capacity and heat content. *J Phys Chem A.* 1998;102(26):5128-41.
9. Li Z, Wang C, Kang W, Li C, Zhang P. Temperature and compression effects on electron heat capacity and electron-phonon coupling in aluminum and beryllium: insights from *ab initio* simulations. *Plasma.* 2015;22. <http://dx.doi.org/10.1063/1.4935843>.
10. Schroeder DV. *An introduction to thermal physics.* 1st ed. New York: Addison-Wesley Professional; 1999. 409 p.
11. Mizutani U, Kamiya A. Electronic specific heat measurements for quasicrystals and Frank-Kasper crystals in Mg-Al-Ag, Mg-Al-Cu, Mg-Al-Zn, Mg-Ga-Zn and Al-Li-Cu alloy systems. *J Phys Condens Matter.* 1991;3(21):3711-8.
12. Inden G. Computer calculation of the free energy contribution due to chemical and/or magnetic ordering. In: *Proc. Project Meeting CALPHAD; 1976; Dusseldorf. Proceedings.* Dusseldorf: Dusseldorf Inst.; 1976. pp. 1-13.
13. Hillert M, Jarl M. A model for alloying in ferromagnetic metals. *Calphad.* 1978;2(3):227-38.
14. Chuang Y, Schmid R, Chang YA. Magnetic contributions to the thermodynamic functions of pure Ni, Co and Fe. *Metall Trans, A, Phys Metall Mater Sci.* 1985;16(2):153-65.
15. Li Z, Mao H, Selleby M. Thermodynamic modeling of pure Co accounting two magnetic states for the Fcc phase. *J Phase Equilibria Diffus.* 2018;39(5):502-9.
16. Ferreira IL, Garcia A. The application of numerical and analytical approaches for the determination of thermophysical properties of Al-Si-Cu-Mg alloys. *Contin Mech Thermodyn.* 2020;32:1231-44.
17. Ferreira IL, Castro JA, Garcia A. Determination of heat capacity of pure metals, compounds and alloys by analytical and numerical methods. *Thermochim Acta.* 2019;682:178418.
18. Jácome PAD, Landim MC, Garcia A, Furtado AF, Ferreira IL. The application of computational thermodynamics and a numerical model for the determination of surface tension and Gibbs Thomson coefficient of aluminum based alloys. *Thermochim Acta.* 2011;523(1-2):142-9.
19. Clyne TW, Kurz W. Solute redistribution during solidification with rapid solid state diffusion. *Metall Trans, A, Phys Metall Mater Sci.* 1981;12(6):965-71.
20. Brody HB, Flemings MC. Solute redistribution during solidification. *Trans Metall Soc AIME.* 1966;236:615-24.
21. Voller VR. On a general back-diffusion parameter. *J Korean Cryst Growth Cryst Technol.* 2001;226(4):562-8.
22. Erol M, Marasli N, Böyük U. Determination of anisotropy of Crystal-melt interfacial energy from the observed grain boundary groove shapes at multiple orientations. *Surf Rev Lett.* 2009;16(4):579-88.
23. Prokofjev SI. Estimations of grain-boundary surface tension in elemental solids. *J Mater Sci.* 2017;52(8):4265-77.
24. Souza M, Paupitz R, Seridonio A, Lagos R. Specific heat anomalies in solids described by a multilevel model. *Braz J Phys.* 2016;46(2):206-12.
25. Snider E, Dasenbrock-Gammon N, McBride R, Debessai M, Vindana H, Vencatasamy K, et al. Room-temperature superconductivity in a carbonaceous sulfur hydride. *Nature.* 2020;586(7829):373-7.
26. Larsson S. Effect of pressure on superconducting properties. *J Supercond Nov Magn.* 2015;28(6):1693-8.
27. George PK, Thompson ED. The Debye temperature of Nickel from 0 to 300K. *J Phys Chem Solids.* 1967;28(12):2539-44.
28. Zalden P, Siegert KS, Rols S, Fischer HE, Schlich F, Hu T, et al. Specific heat of (GeTe)<sub>x</sub>(Sb<sub>2</sub>Te<sub>3</sub>)<sub>1-x</sub> phase-change materials: the impact of disorder and anharmonicity. *Chem Mater.* 2014;26(7):2307-12.
29. Giauque W, Meads J. The heat capacities and entropies of Aluminum and Copper from 15 to 300°K. *J Chem Phys.* 1941;63:423-32.
30. Brooks CR, Bingham RE. The specific heat of aluminum from 330 to 890 K and contributions from the formation of vacancies and anharmonic effects. *J Phys Chem Solids.* 1968;29(9):1553-60.
31. Valencia JJ, Quedest P. Thermophysical properties. In: *ASM International. ASM handbook: casting.* Ohio: ASM International; 2008. p. 468-81. (vol. 15).
32. Cristescu S, Simon F. Specific heat of beryllium, germanium, and hafnium at low temperatures. *Z Phys Chem, B Chem Elem Proz Aufbau Mater.* 1934;25:273.
33. Howe SD, O'Brien RC, Ambrosi RM, Gross B, Katalenich J, Sailer L, et al. The Mars Hopper: an impulse-driven, long range, long-lived mobile platform utilizing in-situ Martian resources. *Acta Astronaut.* 2011;69(11-12):1050-6.
34. Kelley KK. The specific heat of pure iron at low temperatures. *J Chem Phys.* 1943;11(1):16-8.
35. Eucken A, Werth H. Die spezifische wärme einiger metalle und metallegierungen bei tiefen temperaturen. *Zeits f anorg Allgem Chemie.* 1930;188:152-72.
36. Simon F, Swain RL. Untersuchungen über die spezifische Wärme bei tiefen temperaturen. *Z Phys Chem, B Chem Elem Proz Aufbau Mater.* 1935;28B:189-98.
37. Smithells CJ. General physical properties. In: Brandes EA, Brook GB, editors. *Metals reference book.* 7th ed. Amsterdam: Butterworth-Heinemann; 1992.
38. Mills KC. Recommended values of thermophysical properties for selected commercial alloys. Cambridge: Woodhead Publishing; 2002.
39. Gaskell DR. *Introduction to metallurgical thermodynamics.* New York: McGraw-Hill; 1973. p. 497-501.
40. Awbery JH, Griffiths E. The thermal capacity of pure iron. *Proc R Soc Lond A Math Phys Sci.* 1940;174(956):1-15.
41. Pankratz LB, Mrazek RV. *Thermodynamic properties of elements and oxides.* Washington: US Bureau of Mines; 1982.
42. Desai PD. Thermodynamic properties of nickel. *Int J Thermophys.* 1987;8(6):763-80.
43. Kohlhaas R, Dünner PH, Schmitz-Pranghe N. Über die Temperaturabhängigkeit der Gitterparameter von Eisen, Kobalt und Nickel im bereich hoher temperaturen. *Z Angew Phys.* 1967;23:245-9.
44. Sankovich AM, Markin AV, Smirnova NN, Zvereva IA. Heat capacity and the thermodynamic properties of layered perovskite-like oxides K<sub>2</sub>La<sub>2</sub>Ti<sub>3</sub>O<sub>10</sub> and K<sub>2</sub>Nd<sub>2</sub>Ti<sub>3</sub>O<sub>10</sub>. *Russ J Phys Chem.* 2019;93(3):407-16.